

Superfluid-Mott transition and thermal phases of correlated lattice bosons: a classical fluctuation theory

Abhishek Joshi and Pinaki Majumdar

Harish-Chandra Research Institute, HBNI, Chhatnag Road, Jhusi, Allahabad 211019

(Dated: April 6, 2024)

We present a method that generalises the standard mean field theory of correlated lattice bosons to include amplitude and phase fluctuations of the $U(1)$ field that induces onsite particle number mixing. This arises formally from an auxiliary field decomposition of the kinetic term in a Bose Hubbard model. We solve the resulting problem, initially, by using a classical approximation for the particle number mixing field and a Monte Carlo treatment of the resulting bosonic model. In two dimensions we obtain T_c scales that dramatically improve on mean field theory and are within about 20% of full quantum Monte Carlo estimates at density $n = 1$. The ‘classical approximation’ ground state, however, is still mean field, with an overestimate of the critical interaction, U_c , for the superfluid to Mott transition. By further including low order quantum fluctuations in the free energy functional we improve significantly on the U_c , and the overall thermal phase diagram. The classical approximation based method has a computational cost linear in system size. The methods readily generalise to multispecies bosons, disorder, and the presence of traps, and yield real frequency response functions.

I. INTRODUCTION

The experimental realization^{1–4} of a quantum phase transition from a superfluid to a Mott insulator for bosons in an optical lattice bridged the gap^{5,6} between condensed matter and cold atom physics. The quantitative features of the transition are captured by quantum Monte Carlo (QMC) simulations in both two dimensions⁷ and three dimensions⁸. These have established the phase diagram involving, (i) the interaction, U , driven superfluid to Mott insulator transition in the ground state at integer filling, and (ii) the thermally driven superfluid to normal Bose liquid transition.

While QMC provides high accuracy numerical results for the thermodynamic features, one would want methods that (i) shed light on the key physical effects, and (ii) allow access to dynamical properties. Mean field theory^{9,10}, although quantitatively not very accurate, highlights the crucial effect of particle number fluctuation in the superfluid ground state. More sophisticated methods, *e.g.*, strong coupling expansion^{11,12}, variational calculations¹³, the projection operator technique¹⁴, cluster gutzwiller¹⁵ and variational cluster schemes^{16,17} improve on the mean field ground state and yield results that agree well with QMC for the zero temperature transition.

There is less insight into the finite temperature situation. Mean field theory has a finite temperature generalisation but leads to a large overestimate of T_c scales. Slave particle methods^{18,19} and a self consistent standard basis operator²⁰ approach have been used to study the thermal physics. Recently a bosonic version of dynamical mean field theory^{21–23} (BDMFT) has been developed - retaining all local quantum fluctuations but ignoring spatial correlations. Among the methods above only the results of BDMFT compare reasonably with QMC in terms of thermal properties.

We present an alternate extension of mean field theory in this paper, with emphasis on *spatial fluctuations*, which we believe are important in lower dimensions, and include temporal (quantum) fluctuations only approximately. The two versions of this approach are, borrowing from the nuclear physics

literature,^{28–30} (i) the static path approximation (SPA), and (ii) the perturbed static path approximation (PSPA), for the functional integral defining the partition function. We present the analytic basis of these methods and obtain the following results for the two dimensional (2D) Bose Hubbard model within a Monte Carlo implementation of these schemes.

(i) Ground state: at zero temperature the SPA expectedly reproduces the mean field phase boundary between the superfluid and the Mott insulator. PSPA results are almost indistinguishable from full QMC.

(ii) Thermal scales: at filling $n = 1$ both SPA and PSPA lead to a maximum superfluid T_c that is $T_c^{max} \sim 2.5t$ (where t is the hopping scale). Within QMC $T_c^{max} \sim 2t$ while mean field theory predicts $T_c^{max} = 6t$, see Fig. 1.

(iii) Number fluctuations: we establish the distribution of

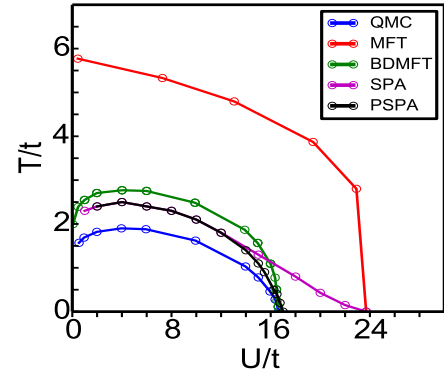


FIG. 1. Color online: Superfluid T_c from different methods for the 2D Bose Hubbard model at filling $n = 1$. We use $U_c(0)$, the $T = 0$ critical interaction, and T_c^{max} , the maximum superfluid T_c , to characterise each scheme. (i) Mean field theory (MFT) yields $U_c(0) = 24t$ and $T_c^{max} = 6t$, (ii) for BDMFT $U_c(0) \sim 17t$ and $T_c^{max} \sim 3t$, (iii) for our simplest method, the SPA, $U_c(0) = 24t$ and $T_c^{max} \sim 2.5t$, (iv) for the perturbed SPA, $U_c(0) \sim 17t$ and $T_c^{max} \sim 2.5t$. For full quantum Monte Carlo (v) $U_c(0) \sim 17t$ and $T_c^{max} \sim 2t$. The abbreviations are explained in the text.

the key ‘hybridisation’ field that is responsible for on site particle number fluctuations and illustrate spontaneous fluctuations even in the Mott phase at finite temperature

(iv) Spatial correlations: we extract a characteristic length-scale $\xi(T, U)$ for the hybridisation field. ξ diverges as the thermal transition is approached, emphasising that the hybridisation field follows a spatially correlated distribution - not accessible within ‘local’ theories.

(v) Amplitude-vs-phase fluctuations: while both amplitude and phase fluctuations are relevant at small U , the large U low temperature problem is dominated by phase fluctuations - which allows us to construct and benchmark a XY model. This well approximates $T_c(U)$ and provides physical insight.

The rest of the paper is organized as follows: in Section II we discuss our approach and its numerical implementation. Section III discusses our results for the ground state and thermal behaviour. Section IV provides an analysis in terms of an XY model, and discusses computational checks.

II. MODEL AND METHOD

We explore our methods in the context of the 2D Bose Hubbard model at unity filling:

$$H = -t \sum_{\langle ij \rangle} a_i^\dagger a_j - \mu \sum_i n_i + \frac{U}{2} \sum_i n_i(n_i - 1)$$

where a and a^\dagger are the usual second quantised bosonic operators, t is the nearest neighbour hopping amplitude, U is the onsite repulsion, and the boson density is fixed at $n = 1$ by using a chemical potential μ .

In order to arrive at our approximations we follow a standard path integral approach^{25–27}. Within the path integral formalism the full partition function is given by

$$\begin{aligned} Z &= \int \mathcal{D}b \mathcal{D}\bar{b} e^{-(S_0 + S_K)} \\ S_0 &= \int_0^\beta d\tau [\sum_i \bar{b}_i (\partial_\tau - \mu) b_i + \frac{U}{2} \sum_i \bar{b}_i b_i (\bar{b}_i b_i - 1)] \\ S_K &= \int_0^\beta d\tau (-t) \sum_{\langle ij \rangle} (\bar{b}_i b_j + h.c.) \end{aligned}$$

The b 's in the path integral are space and (imaginary) time dependent classical fields. S_0 involves the local terms and S_K the kinetic energy.

We separate the kinetic term as follows: $S_K = S_K^a + S_K^b$,

$$\begin{aligned} S_K^a &= - \sum_{\vec{k}} A_{\vec{k}} \bar{b}_{\vec{k},0} b_{\vec{k},0} \\ S_K^b &= - \sum_{\vec{k}} B_{\vec{k}} \bar{b}_{\vec{k},0} b_{\vec{k},0} - \sum_{n \neq 0, \vec{k}} t_{\vec{k}} \bar{b}_{\vec{k},n} b_{\vec{k},n} \end{aligned}$$

where $A_{\vec{k}} = \theta(t_{\vec{k}}) t_{\vec{k}}$ and $B_{\vec{k}} = \theta(-t_{\vec{k}}) t_{\vec{k}}$ and $t_{\vec{k}} = 2t(\cos k_x a + \cos k_y a)$. Note that S_K^a involves only zero frequency modes of $b_{\vec{k}}$, and only \vec{k} for which the tight binding energy, $-t_{\vec{k}}$, is negative. S_K^b involves the rest of the contributions.

We use a Hubbard-Stratonovich transformation to decouple only S_K^a , keeping S_K^b untouched.

$$e^{-S_K^a} = \int \mathcal{D}\psi \mathcal{D}\psi^* e^{-\sum_{\vec{k}} \psi_{\vec{k}}^* \psi_{\vec{k}} + \sum_{\vec{k}} \sqrt{A_{\vec{k}}} (\psi_{\vec{k}} \bar{b}_{\vec{k},0} + h.c.)}$$

The focus on S_K^a to start with is to retain bounded weight in a sampling process, as we will explain soon. All the terms above can be collected and Fourier transformed back to real space and imaginary time to give us

$$\begin{aligned} Z &= \int \mathcal{D}\psi \mathcal{D}\psi^* \mathcal{D}b \mathcal{D}\bar{b} e^{-(S + S_K^b)} \\ S &= S_0[b, \bar{b}] - \sum_{ij} (C_{ij} \bar{b}_i \psi_j + hc) + \sum_i \psi_i^* \psi_i \\ C_{ij} &= \frac{1}{N} \sum_{\vec{k}} \sqrt{A_{\vec{k}}} e^{i\vec{k}(\vec{r}_i - \vec{r}_j)} \end{aligned}$$

This is an exact representation of Bose Hubbard model. The fourfold symmetric real function C_{ij} is shown in Fig.2, with respect to the reference site i taken at the origin.

We examine two approximations: (i) Drop S_K^b completely and solve for the physics arising from S - this is the SPA for the partition function and treats the hybridising field as classical. (ii) Treat the effect of dynamical fluctuations contained in S_K^b to quadratic order, this is the PSPA.

A. The static path approximation (SPA)

We examine the SPA in detail and relegate the algebra for the PSPA to an Appendix and only provide the final PSPA result here. Within the SPA

$$\begin{aligned} Z &= \int \mathcal{D}\psi \mathcal{D}\psi^* \mathcal{D}b \mathcal{D}\bar{b} e^{-S} \\ &= \int \mathcal{D}\psi \mathcal{D}\psi^* \text{Tr}[exp(-\beta H')] \\ &= \int \mathcal{D}\psi \mathcal{D}\psi^* e^{-\beta F\{\psi\}} \end{aligned}$$

In the expression above

$$\begin{aligned} F &= \sum_i F_i = -\frac{1}{\beta} \sum_i \log(\text{Tr}[exp(-\beta H'_i)]) \\ H'_i &= (a_i^\dagger \Phi_i + h.c) + \frac{U}{2} n_i(n_i - 1) - \mu n_i + \psi_i^* \psi_i \\ \Phi_i &= \sum_j C_{ij} \psi_j \end{aligned}$$

In what follows we will call ψ_i the *auxiliary field*, which is what we actually update, and Φ_i the *hybridisation field*.

The task at any temperature is to sample over configurations of ψ with weight $P[\psi] \propto \prod_i \text{Tr}[e^{-\beta H'_i}]$. The sampling is performed using the Metropolis algorithm. This involves calculating $\text{Tr}[e^{-\beta H'_i}]$, for which we construct the matrix for H'_i in the local occupation number basis, $\sim (a_i^\dagger)^n |0\rangle$, truncated at boson occupancy $N_b = 10$.

We use a local update scheme. The hybridization at any site R_i is given by $\sum_j C_{ij} \psi_j$, so changing ψ_i affects the Φ of all

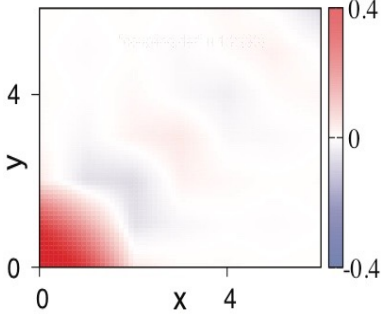


FIG. 2. Color online: The coupling C_{ij} between the boson field b_i and the auxiliary field ψ_j . The reference site i is taken to be the origin $(0,0)$. The plot highlights the rapid decay of C_{ij} with separation R_{ij} , justifying a ‘cluster treatment’ (see text) of the energy cost.

sites on the lattice. However, since C_{ij} falls off quickly with distance we use C_{ij} generated for a cluster of size $N_c = 6 \times 6$, centered around R_i . The free energy required for the update is the sum of F_i on the cluster.

The computational cost of an update is $\propto N_c N_b^3$, where N_c is the cluster size, and N_b^3 is the matrix diagonalisation cost for each site in the cluster. For the system sweep the cost would be $NN_c N_b^3$, where N is the system size. The Monte Carlo method, therefore, is $\mathcal{O}(N)$ with a large prefactor.

After equilibration we store ψ configurations to calculate thermodynamic averages. We adjust μ to remain at unity filling at each temperature. At $T = 0$ where every site sees the same hybridisation SPA reduces to mean field theory. At finite temperature both the amplitude and the phase of the ψ_i (and so the Φ_i) fluctuate.

B. Perturbed static path approximation (PSPA)

To improve the SPA one needs to build back the neglected quantum fluctuations. To derive the corrected form of free energy, we solve the S part exactly and include corrections due to S_K^b perturbatively by summing diagrams with ‘self avoiding’ paths to all order and then replacing the series sum by an exponentiated term. The full partition function is approximated by

$$Z \approx \int \mathcal{D}\psi \mathcal{D}\psi^* e^{-\beta(F+X-Y)}$$

$$F = -\frac{1}{\beta} \log(\text{Tr}[exp(-\beta H')])$$

Here F is the contribution due to S part of the action. The details are given in the Appendix. In the updated scheme sampling over ψ configuration is to be done with weight $P[\psi] \propto e^{-\beta(F+X-Y)}$. X depends upon coupling B_{ij} . Since B_{ij} also falls off very quickly with distance, we use B_{ij} generated for 4×4 lattice. X can be written as sum of contribution coming from onsite, nearest neighbour bonds, and next nearest neighbour bonds for every site whereas Y is sum of contribution from only nearest neighbour bonds.

The change in the free energy, relevant for the update, is computed on a 6×6 cluster centered on the update site. While calculating Y we sum over only the lowest four eigenstates. The rest follows as in SPA.

While we emphasize the PSPA results in this paper, due to its quantitative accuracy, we often compare and contrast it to SPA - given the conceptual simplicity of the SPA scheme.

III. RESULTS

A. The ground state

Fig.3 shows the comparison between ground state obtained using the SPA and PSPA schemes. The value of the uniform hybridisation Φ is zero inside the Mott lobe and increases with increase in t/U . The critical value at the tip of the Mott lobe, is found to be $(t/U)_c = 0.0428$ within SPA, the same as the mean field result. The critical point value is $(t/U)_c = 0.0595$ under PSPA, very close to the QMC value.

Fig.4 compares the SPA and PSPA energy functions for uniform hybridisation. Numerical data are shown by open circles, at $U/t = 10, 15, 16$ and 18 , and even order polynomial fits to them are shown by firm lines. The minimum of the respective function decides the $T = 0$ order parameter within that schemes. In the following discussion we ignore the angle dependence of Φ since it is irrelevant at $T = 0$.

In the $U = 10t - 18t$ window shown the SPA ground state is superfluid. There is a local maximum in $E_{SPA}(\Phi)$ at $\Phi = 0$ and a $\Phi \neq 0$ minimum that moves to smaller value with increasing U/t . The SPA leads to a second order transition from superfluid to Mott insulator at $U/t = 24$.

For the PSPA there is always a minimum at $\Phi = 0$. The $\Phi \neq 0$ minimum is deeper for $U \lesssim 17t$ - leading to a superfluid state. At $U = 18t$, panel (d) in Fig.4, the PSPA minimum at finite Φ is no longer visible. There is a weakly first order SF to Mott transition within the PSPA at $U \sim 17.5t$.

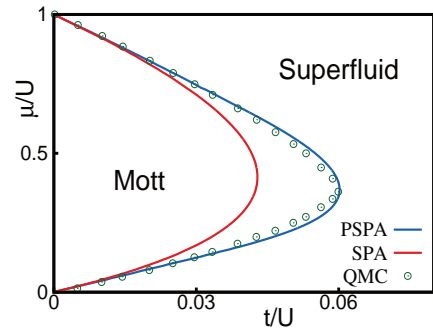


FIG. 3. Color online: The ground state of the 2D Bose Hubbard model for varying μ/t and U/t . The region within the lobe is a Mott insulator with $n = 1$. The inner lobe, with a larger $(t/U)_c$ is the result of the SPA and is the same as in mean field theory. The outer lobe, with smaller $(t/U)_c$, is the result of the PSPA and is indistinguishable from QMC results.

To locate the origin of the difference between SPA and PSPA we analysed the energy functions in terms of their Landau expansion. The SPA energy at $T = 0$ has a Landau expansion of the form: $E_{SPA}(\Phi) = \sum_m a_m \Phi^m$ where Φ is the uniform hybridisation field. Naturally only even powers arise in the expansion. The coefficients a_m can be estimated as

$$\begin{aligned} a_0 &= \frac{U}{2} n(n-1) - \mu n \\ a_2 &= \frac{1}{4} + t G_{ii}(0) \\ a_4 &= -(t^2/4) G_{ii}^{2c} \end{aligned}$$

where $G_{ii}(0) = -\int_0^\beta d\tau \langle T_\tau b(\tau) b^\dagger(0) \rangle$ and

$$G_{ii}^{2c} = \int_0^\beta d\tau_1 \dots d\tau_3 \langle T_\tau b(\tau_1) b(\tau_2) b^\dagger(0) b^\dagger(\tau_3) \rangle - 2\beta G_{ii}^2(0)$$

The G_{ii} are correlators in the $\Phi = 0$ problem.

For PSPA the expansion is similar, of the form $E_{PSPA}(\Phi) = \sum_m a'_m \Phi^m$ but an analytic derivation of the coefficients is more involved and is described in the Appendix.

Fig.5 shows the Landau parameters obtained by fitting the SPA and PSPA energy functions, and the energy difference function $\delta E = E_{PSPA} - E_{SPA}$. For SPA the coefficient a_4 is always positive, a_6 is small and positive, and the SF to Mott transition is driven by a_2 changing from negative to positive. For PSPA $a_2 > 0$ and $a_6 > 0$ throughout. There is

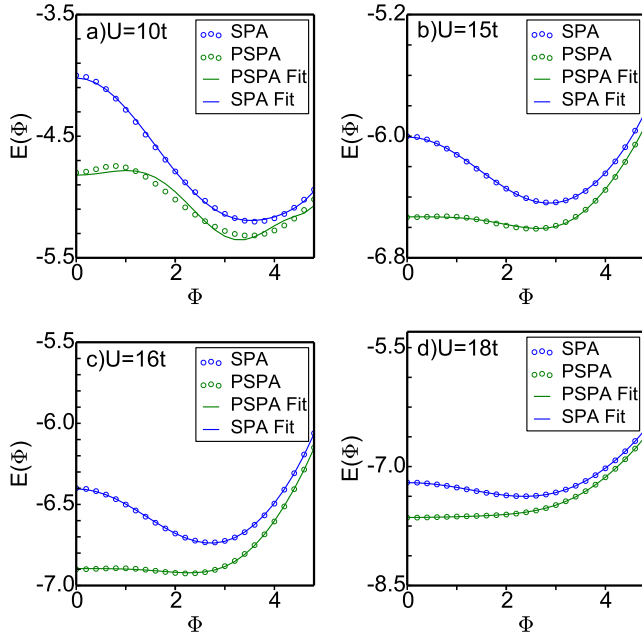


FIG. 4. Color online: The open circles in panels (a)-(d) show the SPA and PSPA energy functions, plotted for a uniform order parameter, Φ , for the values of U/t indicated. The SPA and PSPA minima match with each other in panels (a) and (b), in panel (c) the difference is noticeable, while in (d) the SPA minimum is at finite Φ while the PSPA minimum has shifted to zero. The firm lines are even order Landau fits to the SPA and PSPA functions upto $|\Phi|^6$

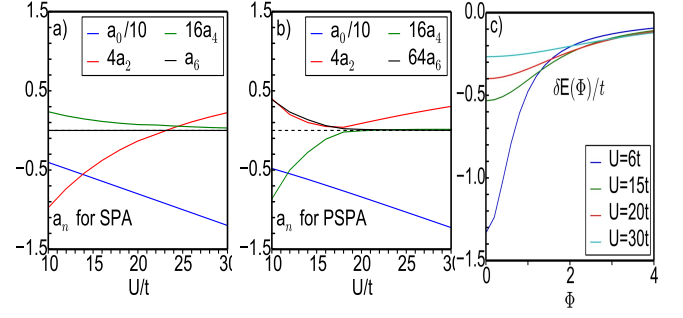


FIG. 5. Color online: (a) Landau parameters for SPA and (b) Landau parameters for PSPA. Note that a_4 remains positive for all U/t in SPA, a_6 is negligible, and the second order transition is driven by sign change in a_2 . For PSPA a_2 remains positive at all U/t , so there is always a minimum at $\Phi = 0$, and the transition is driven by a_4 becoming less negative with growing U/t . a_6 remains positive. (c) Shows the behaviour of $E_{PSPA} - E_{SPA}$, highlighting the source of the large positive a_2 and the negative a_4 in PSPA.

always a minimum at $\Phi = 0$. a_4 is large and negative at small U/t , generating the SF minimum. With increasing U/t the coefficient $a_4 \rightarrow 0$ and the finite Φ minimum becomes higher in energy than the $\Phi = 0$ minimum. This drives a weak first order SF to Mott transition. Panel (c) shows δE , and the data reveals the origin of the difference in the a_2 and a_4 coefficients between SPA and PSPA.

We found a slight disagreement between fit parameters and the analytic estimate for coefficients of SPA functional: a_0 and a_2 match well but a_4 deviates when $(U_c - U) \gg t$.

B. Thermal behaviour

1. Indicators

We track the following indicators to locate the thermal transition and also quantify the amplitude and phase fluctuations in the problem.

(i) The structure factor: $S(\mathbf{q}) = \frac{1}{N^2} \sum_{ij} \Phi_i \Phi_j^* e^{i\mathbf{q} \cdot (\vec{r}_i - \vec{r}_j)}$ The T_c is extracted from the T dependence of the $S(0, 0)$.

(ii) The momentum distribution of bosons,

$$\langle n(\vec{k}) \rangle = \frac{1}{N} \left\langle \sum_{i,j} e^{-i\vec{k} \cdot (\vec{r}_i - \vec{r}_j)} \text{Tr}[e^{-\beta H'} a_i^\dagger a_j] \right\rangle$$

(iii) The distribution, and moments, of the hybridisation field:

$$P(|\Phi|) = \frac{1}{NN_\alpha} \sum_{\alpha,i} \delta(|\Phi| - |\Phi_i^\alpha|)$$

where α is a configuration label and N_α the number of configurations averaged over. Note that P is normalised. The distribution allows us to calculate the moments $\langle y^n \rangle = \int dy P(y) y^n$ where $y = |\Phi|$. $n = 1$ yields the mean, $\langle \Phi_{av} \rangle$. We compute the standard deviation, or ‘width’ of the $|\Phi|$ as $\Phi_{wid} = \sqrt{\langle |\Phi|^2 \rangle - \langle |\Phi| \rangle^2}$.

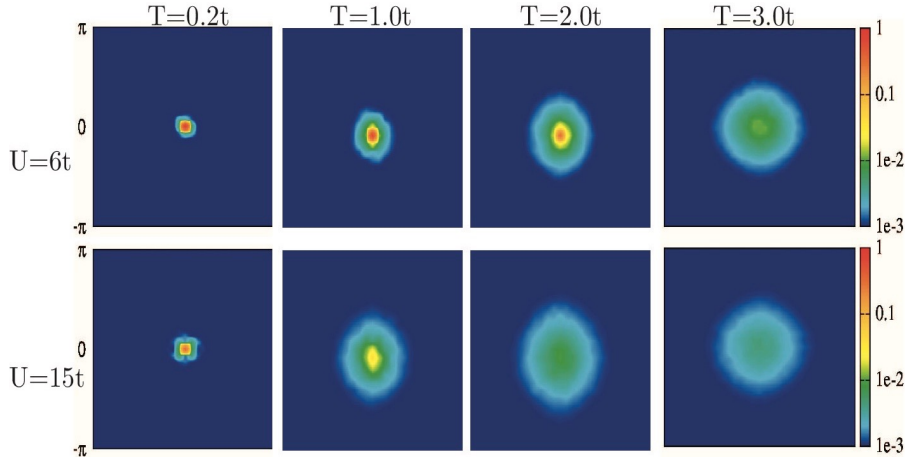


FIG. 6. Color online: The momentum distribution, $n_{\mathbf{k}} = \langle \langle a_{\mathbf{k}}^\dagger a_{\mathbf{k}} \rangle \rangle$, for varying interaction strength and temperature in the superfluid phase. The intensity scale is logarithmic to simultaneously capture the condensate peak in the superfluid state and show the particle distribution in high temperature normal phase.

(iv) The spatial correlation in a single Monte Carlo snapshot:

$$C_i = \sum_{\delta} |\Phi_i| |\Phi_{i+\delta}| \cos(\theta_i - \theta_{i+\delta})$$

where δ are the nearest neighbours of i .

(v) Finally, we compute a correlation length $\xi(U, T)$ from a fit to the structure factor data: $\xi(T, U) = \frac{1}{2\sin(\pi/L)} \sqrt{\frac{S(0,0)}{S(2\pi/L,0)} - 1}$

2. Thermal phase diagram

We now turn to the thermal phase diagram shown in Fig.1 and discuss it in more detail. The figure compares the $T_c(U)$ obtained from SPA and PSPA with mean field theory, bosonic DMFT, and full QMC. The SPA T_c is already a significant improvement over mean field theory and compares reasonably with QMC in the intermediate U/t regime. The T_c of the superfluid should vanish as $U \rightarrow 0$ since there is no phase stiffness in the absence of interactions. We do obtain a non monotonic dependence of T_c on U/t with a maximum located at $U/t \sim 4$, consistent with QMC, but the $U/t \rightarrow 0$ limit is not captured correctly. The PSPA scheme leads to T_c 's that are close to the SPA results for $U/t \lesssim 14$, beyond which the PSPA T_c quickly drops to zero. However even PSPA does not correctly capture the asymptotic behaviour as $U/t \rightarrow 0$.

We will show detailed results for four representative U/t values: (i) $U = 6t$ where the system is a moderate coupling superfluid, (ii) $U = 15t$ where it is a strongly interacting superfluid, (iii) $U = 20t$ - a 'weak Mott state', just beyond U_c , and (iv) $U = 30t$ - a deep Mott state. We highlight spatial maps and distributions at four temperatures, $T = 0.2t, t, 2t$ and $3t$. We first discuss the two superfluid regimes in the next subsection, and the two Mott states in the subsection after.

3. The superfluid phase

At $T = 0$ in the superfluid the hybridisation field is uniform. The occupation at $T = 0$ consists of a peak at $\vec{k} = (0, 0)$ and a \vec{k} independent occupancy at $\vec{k} \neq (0, 0)$. The $\vec{k} = (0, 0)$ occupancy, N_0 , falls with increasing U/t in the ground state, becoming $\mathcal{O}(1)$ for $U > U_c$. Fig.6 shows our result for the momentum distribution at $U = 6t$ and $U = 15t$ for varying temperature. We show the quantitative behaviour in Fig.7, but Fig.6 already reveals that the $\vec{k} = (0, 0)$ occupancy falls with T and U , and at a given T the 'cloud' at $U = 15t$ is always broader than the cloud at $U = 6t$.

Fig.7 quantifies features of the finite T behaviour. Panels (a) and (b) show the momentum dependence of the occupancy along the diagonal $(0, 0) \rightarrow (\pi, \pi)$. The occupancy, plotted on a log scale, suggests that there is an exponential fall off at low \vec{k} in the low T regime, tailing off to a finite \vec{k} independent occupancy at large momentum. Crudely, the T dependence

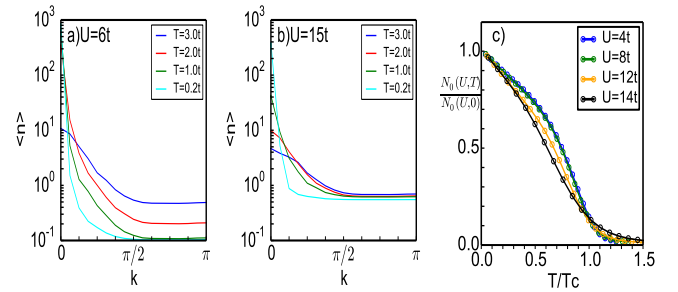


FIG. 7. Color online: The temperature dependence of the $\vec{k} = 0$ occupancy of bosons for varying U . The plot, normalising the occupancy with respect its $T = 0$ value and the temperature with respect to $T_c(U)$ leads to an approximately 'universal' result. This, despite the varying mix of amplitude and phase fluctuations as U varies from weak to strong coupling.

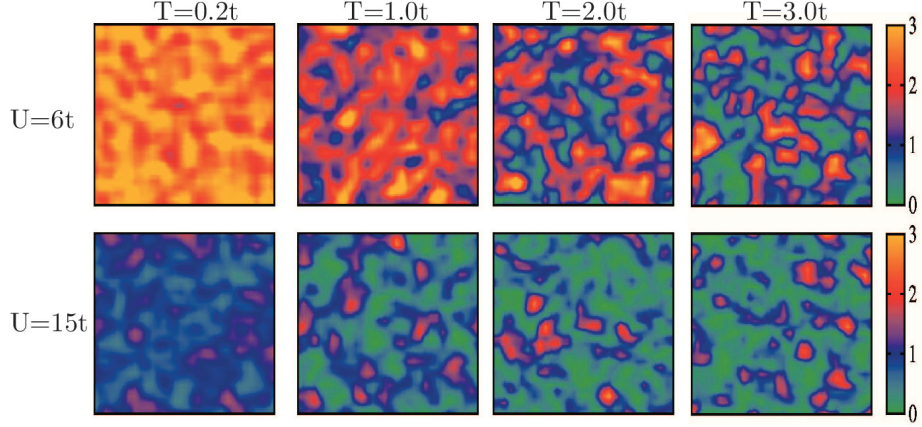


FIG. 8. Color online: Snapshot of spatial correlations in the superfluid regime. The maps indicate the correlation C_i of the hybridisation $\Phi_i = |\Phi_i|e^{i\theta_i}$ at a site with its four neighbours. $C_i = \sum_{\delta} |\Phi_i| |\Phi_{i+\delta}| \cos(\theta_i - \theta_{i+\delta})$. Notice the quasi homogeneous pattern at low T in both the rows. The connected pattern begins to fragment with increasing T . However, even for $T > T_c$ small spontaneous clusters with large correlation are present. System size 32×32 .

seems to follow the form

$$\langle n(\vec{k}) \rangle_T \sim n_{\infty}(T) + n_0(T) f(k/\bar{k}(T))$$

where $n_{\infty}(T)$ is the occupancy of the large momentum states, $n_0(T)$ is the occupancy of the $(0,0)$ state, and $\bar{k}(T) \rightarrow 0$ as $T \rightarrow 0$. The function $f(x) \rightarrow 0$ as $x \rightarrow \infty$ and $f(x) \rightarrow 1$ as $x \rightarrow 0$. Panel (c) indicates that the occupancy of the $\vec{k} = (0,0)$ mode follows an approximate behaviour: $\frac{N_0(U,T)}{N_0(U,0)} \approx h(\frac{T}{T_c(U)})$ where $h(x)$ can be inferred from Fig.7(c).

Fig.8 shows the correlation C_i for single Monte Carlo snapshots, at $U = 6t$ (top) and $U = 15t$ (bottom). At the lowest temperature shown there is only weak amplitude and angular fluctuation, hence C_i is only weakly inhomogeneous. The second column, $T = t$, corresponds to $\sim 0.5T_c$ at $U = 6t$ but is above T_c at $U = 15t$. As a result the top panel still shows a connected pattern while the $U = 15t$ case shows only small correlated droplets in an otherwise uncorrelated background.

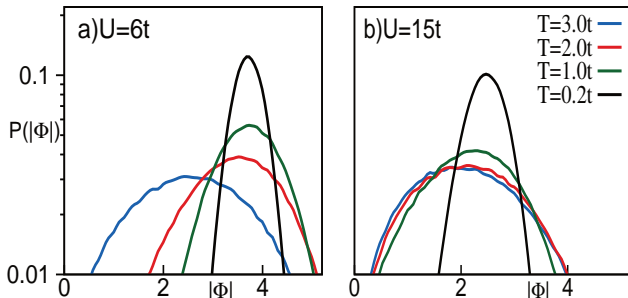


FIG. 9. Distribution of the magnitude of the local hybridisation. Panels (a)-(b) have a superfluid ground state. The lowest temperature in the data set is $T = 0.2t$ at which amplitude fluctuations are already visible. The distributions appear Gaussian in the weaker U systems. A later figure shows the mean and variance of these distributions.

The trend continues to higher T , with the correlation length for $U = 6t$ (which we show later) being larger than that for $U = 15t$ at a given temperature.

We have analysed the auxiliary field backgrounds in detail. Fig.9(a) and 9(b) shows the distribution $P(|\Phi|)$ in the superfluid regime. At $T = 0$ the $|\Phi|$ is homogeneous across the system and the distribution is a delta function. At finite T we see that $\log P(|\Phi|)$ has a parabolic character, $\sim A(T) - (|\Phi| - \bar{\Phi}(T))^2/B(T)$, where $A(T)$ is a normalisation constant, $\bar{\Phi}(T)$ refers the amplitude with maximum probability, and $B(T)$ is a measure of the width of the distribution. As is obvious from the plots, for the SF $\bar{\Phi}(T)$ falls with increasing T , while $B(T)$ rises from zero as T increases. By the time $T \sim T_c$ for both the weak and strongly interacting superfluids the width of the distribution is comparable to the mean. Amplitude fluctuations are significant all across the high T superfluid.

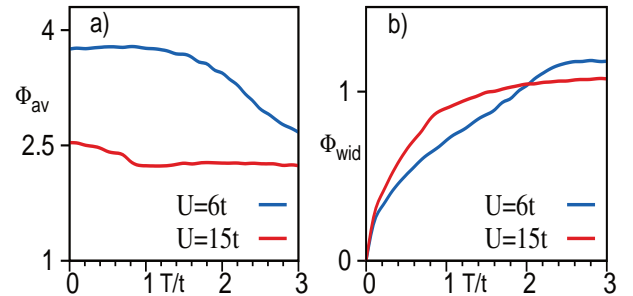


FIG. 10. Color online: (a) mean and (b) standard deviation of the magnitude of the hybridisation field. In the superfluid ($U/t \lesssim 16$) the mean falls only weakly between $T = 0$ and T_c , and somewhat faster for $T \gtrsim T_c$. The magnitude fluctuation ‘width’ vanishes in all cases as $T \rightarrow 0$, and grows to a value comparable to the mean by $T \sim 3t$.

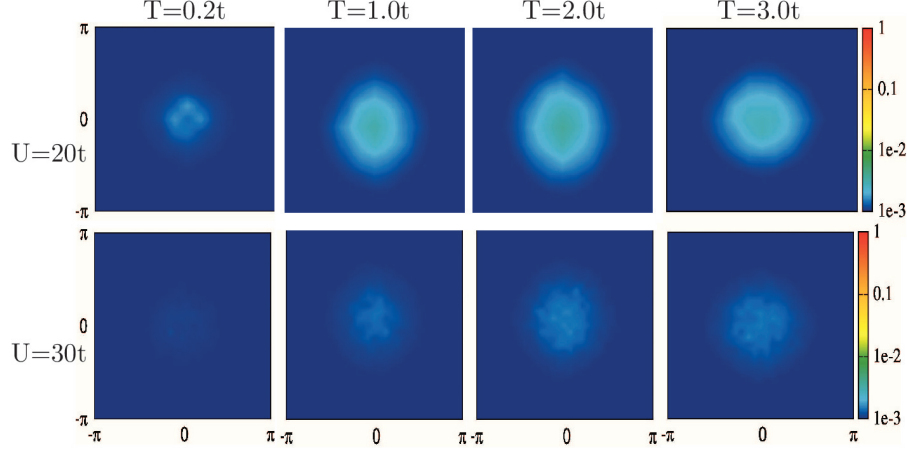


FIG. 11. Color online: The momentum distribution, $n_{\mathbf{k}} = \langle a_{\mathbf{k}}^\dagger a_{\mathbf{k}} \rangle$, for varying interaction strength and temperature in the Mott phase. The intensity scale is logarithmic. We show the thermally excited pattern in the Mott insulator for $U = 20t$ (a weak Mott insulator) and $U = 30t$ (a strong Mott insulator) in the two rows respectively.

Fig.10 shows the detailed T dependence of the mean and width of the distributions, computed from the moments. For the weak coupling SF, with $T_c \sim 2t$, the mean value starts dropping sharply as $T \rightarrow T_c$, and the width at T_c , in Fig.10(b), is ~ 0.5 the mean value. In the strong coupling case, where $T_c \sim t$, the mean value at $T \gtrsim T_c$ is within 20% of the $T = 0$ value, although the width is comparable to the weak coupling case. The width, both at $U = 6t$ and $15t$, behaves $\propto \sqrt{T}$ at low temperature.

4. The Mott insulator

Fig.11 shows the occupancy $\langle n(\vec{k}) \rangle$ of bosons in the weak Mott insulator, $U = 20t$ (top), and the deep Mott insulator, $U = 30t$ (bottom). At $T = 0$ the hybridisation is zero at all sites in the Mott insulator and $\langle n(\vec{k}) \rangle$ is flat over the Brillouin zone. With increase in T , however, a certain structure becomes visible in the momentum dependence. A weak peak

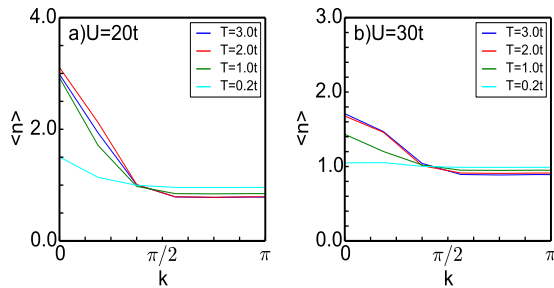


FIG. 12. Color online: The momentum occupation in the Mott state for varying temperature for a momentum scan from $\vec{k} \rightarrow (0,0)$ to (π, π) . The occupancy is $\mathcal{O}(1)$ and shows a weak momentum dependence in the finite T Mott insulator.

emerges near $\vec{k} = (0,0)$ and this feature broadens and picks up intensity at higher temperature. This sequence is prominent in the Mott insulator at $U = 20t$ than in the deep Mott state at $30t$.

This effect arises from the hybridisation field Φ_i being generally non zero at all sites at finite T , following a Boltzmann distribution, and having short range spatial correlation. In the next two figures we show the features of the amplitude distribution - which would be just $\Phi_i = 0$ within mean field theory - and discuss the spatial correlations later.

Fig.12 shows the momentum occupancy along the diago-

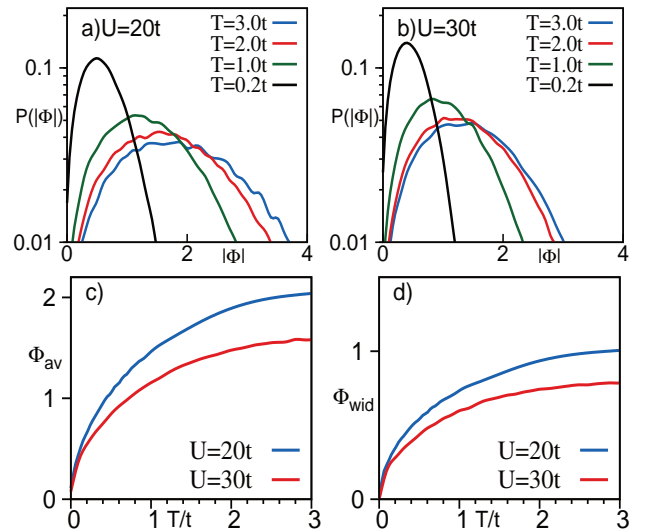


FIG. 13. (a)-(b) Distribution of $|\Phi|$ in the Mott insulator. The lowest temperature is $T = 0.2t$ at which amplitude fluctuations are already visible. (c) Mean and (d) standard deviation of $|\Phi|$. In the Mott phase the mean is zero at $T = 0$ but rises quickly attaining a value ~ 0.5 that of the weak U superfluid at $T \sim 3t$. The width grows as \sqrt{T} , to a value comparable to the mean by $T \sim 3t$.

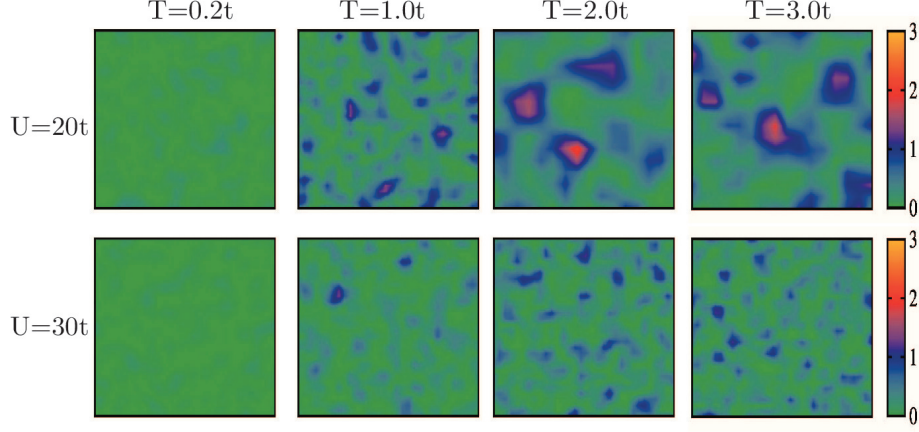


FIG. 14. Color online: Spatial map indicating the correlation C_i of the hybridisation $\Phi_i = |\Phi_i|e^{i\theta_i}$ at a site with its four neighbours. $C_i = \sum_{\delta} |\Phi_i| |\Phi_{i+\delta}| \cos(\theta_i - \theta_{i+\delta})$. Notice the vanishingly small C_i in the low T Mott insulator. The Mott insulator also develops small correlated patches with increasing T . System size 32×32 .

nal scan $(0, 0) \rightarrow (\pi, \pi)$ in the Mott phase for varying T . The $T = 0$ occupancy within our approximation is flat, the $|\Phi_i|$ being zero at all sites. At finite T the thermally induced hybridisation have a spatially correlated pattern, shown later in Fig.14, which leads to a spatially modulated G_{ii} in the Monte Carlo configurations. The nanoscale ‘phase correlated’ patches lead to the weak peak observed in $\langle n(\vec{k}) \rangle$ at small k . The effect expectedly weakens with growing U/t .

Fig.13(a)-(b) shows the distribution of hybridisation for $U = 20t$ and $U = 30t$ while Fig.13 shows the evolution of Φ_{av} and Φ_{wid} with temperature. In the Mott phase the hybridisation is zero at zero temperature. With rise in temperature $P(\Phi)$ picks up weight at non zero Φ . In panels (c)-(d) both the mean and variance of Φ grow as T^α with $\alpha \sim 0.5$. The finite temperature Mott state has thermally induced particle number fluctuations. The increase in interaction strength leads to suppression of number fluctuations.

Fig.14 shows snapshots showing C_i , the correlation of the hybridisation at R_i with its four neighbours in the Mott phase. At $T = 0$ all $C_i = 0$. At finite T there are thermally generated Φ_i , following the distribution shown in Fig.13, that correlated via a coupling that we describe in the next section. Since the fluctuation induced amplitudes are unlikely to be simultaneously large over a wide neighbourhood the patches are small and randomly distributed.

IV. DISCUSSION

A. Analysing the thermal transition

Since the thermal behaviour of SPA and PSPA are similar for U not too close to U_c we focus on the simpler SPA scheme to suggest a mechanism for the thermal transition.

The Landau expansion of the SPA functional, assuming a

homogeneous order parameter, Φ , has the form

$$E(\Phi) = a_0 + a_2|\Phi|^2 + a_4|\Phi|^4$$

as we have already seen. The coefficients a_n depend on $\{U, \mu\}$ and lead to the minimised value $\Phi_0(U) = 0$ for $U > 24t$ at $n = 1$. A similar result, with shifted U_c holds for PSPA. The general finite T form, where the $\Phi_i = \sum_j C_{ij} |\psi_j| e^{i\theta_j}$ has to be treated like a field, can be obtained via a cumulant expansion of the free energy shown in the Appendix. This has the general $U(1)$ invariant form in terms of ψ :

$$F\{\Phi\} = F_0 + F_2 + F_4 + ..$$

$$F_0 = F\{\psi = 0\}$$

$$F_2 = \sum_{ij} f_{2,ij} |\psi_i| |\psi_j| \cos(\theta_i - \theta_j)$$

$$F_4 = \sum_{ijkl} f_{4,ijkl} |\psi_i| |\psi_j| |\psi_k| |\psi_l| g(\theta_i, ..\theta_l)$$

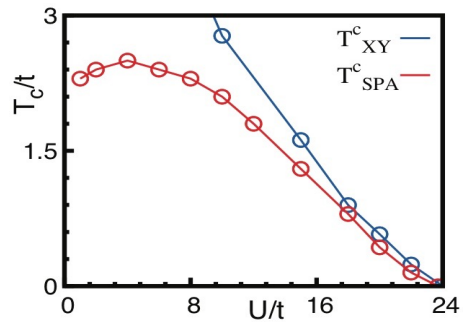


FIG. 15. Comparison of T_c obtained from the effective XY model with T_c from the SPA based Monte Carlo. For $U \gtrsim 0.5U_c$, the match is reasonable, at smaller U amplitude fluctuations are significant.

The coefficients f can be calculated in a hopping expansion.

To capture the qualitative physics we simplify as follows: (i) We drop the fluctuation of the amplitudes with T , treating them as $\psi_0(U) = \Phi_0(U)/2$, the mean field value at $T = 0$. This is consistent with our result for the finite T mean Φ . So, we replace all $|\psi_i|$ by Φ_0 . (ii) We drop the spatial dependence of the $g(\theta_i, \dots \theta_i)$ term. After this, the only variables in F are in F_2 , and the only relevant fluctuations are in the phase θ_i , as in the XY model.

The effective model in this approximation becomes:

$$F\{\Phi\} = \sum_{ij} f_{2,ij} \Phi_0^2 \cos(\theta_i - \theta_j)$$

The function f_2 has a spatial dependence, which we call a_{ij} , and an overall prefactor α that depends on U/t , μ/t , i.e. $f_{2,ij} = \alpha a_{ij}$. This leads to a XY model

$$F\{\theta\} = -J \sum_{ij} a_{ij} \cos(\theta_i - \theta_j)$$

where $J = \alpha(U/t, \mu/t) \Phi_0^2(U/t, \mu/t)$. The T_c would be controlled by J and the spatial character of a_{ij} (which depends only on the bandstructure). In Fig.15. we show a comparison of T_c obtained from the XY model above with the actual T_c within the SPA scheme. Beyond $U \gtrsim U_c/2$ the two results match reasonably.

Fig.16(a) shows the spatial correlation scale $\xi(T, U)$ extracted from an analysis of the \mathbf{q} dependence of the structure factor about $\mathbf{q} = (0, 0)$. This analysis is done for the results obtained using SPA method since at large U/t ratio thermal transition scales are well captured by XY model.

We show the comparison of ξ for various U values with XY model. For XY model change in spatial correlation scale is negligible for system size greater than $L = 32$. We observe that ξ for large U values near the U_c matches with XY result near T_c but high temperature behaviour do not match with XY model. We also find correlation scale(ξ) falls with decrease in interaction.

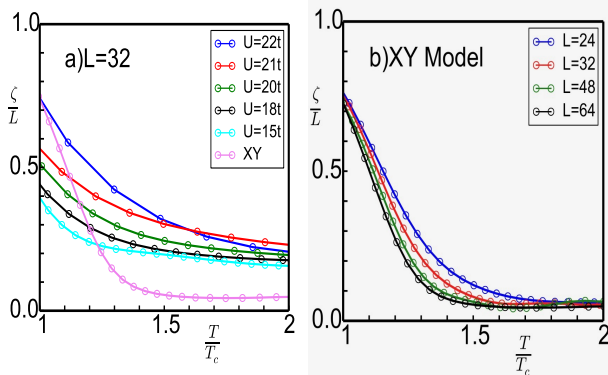


FIG. 16. (a) Comparison of correlation scale $\xi(T)/L$ inferred from our Bose Hubbard results, plotted with respect to $T/T_c(U)$, with $\xi(T)/L$ inferred from the nearest neighbour classical XY model. (b) The system size dependence $\xi(T)/L$ for the classical XY model, showing that the qualitative features do not vary much in the $L = 24$ to $L = 32$ window.

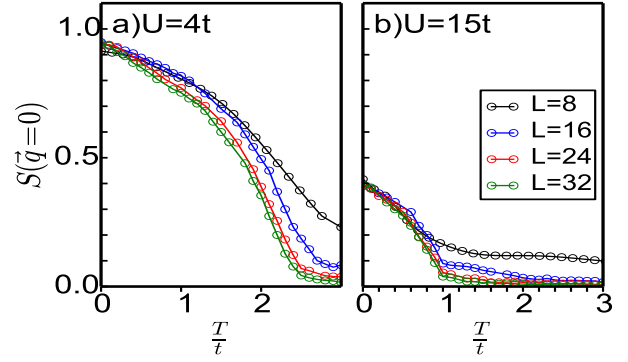


FIG. 17. Size dependence of the $\mathbf{q} = (0, 0)$ structure factor at $U = 4t, 15t$. At both these U values the function, and the superfluid onset temperature is almost size independent for $L \gtrsim 24$.

We came across another real space scheme known as bosonic auxiliary-field Monte Carlo method³¹. They have used this method to study hard core bosons on square and triangular lattice.

B. Size dependence of our results

Fig.17 shows the size dependence of our results. We did the calculation for four system sizes $L = 16, 24, 32, 40$ for SPA and $L = 16, 24, 32$ for PSPA scheme and show the SPA results for the ordering feature in the structure factor. We find that in the superfluid phase, even at moderate coupling ($U = 4t$), a system size $L = 24$ is large enough to probe ‘bulk’ behaviour. $L = 32$ is hard to distinguish from $L = 24$. For larger interaction strength, $U \gtrsim 15t$, $L = 16$ seems capture the behaviour reasonably. This is related to the behaviour of the correlation length $\xi(T, U)$ shown in Fig.16.

C. Results in three dimensions

We have studied the zero temperature SPA and PSPA theory in the case of 3D Bose Hubbard model. At zero temperature we computed the superfluid Mott boundary for unity filling. The SPA result, as in 2D, matches with mean field theory, while the PSPA critical point is almost indistinguishable from the QMC result. We have not checked the finite temperature results in case of 3D but believe our thermal scales would lie within 20% of QMC results.

D. Extensions of the method

Our technique is general enough to handle any kind of diagonal disorder as in case of diagonal disorder the only change is in the exactly handled local Hamiltonian. We can also handle hopping disorder through a change in coupling between the auxiliary field and the bosons. We can of course handle smooth potentials like traps. We can also study spin-orbit

coupling or artificial gauge fields in multispecies bosons as we will separately report. Finally, given the equilibrium classical backgrounds we can compute Green's functions of the Bose theory via a strong coupling expansion. We will present results on this soon.

V. CONCLUSIONS

We have computed the phase diagram of the two dimensional Bose Hubbard model at integer filling. The results, based on a classical approximation to the 'hybridisation field', and a quantum correction on it, yield transition scales, $T_c(U)$, that compare favourably with full quantum Monte Carlo results. The simpler version of the method, called SPA, has a computational cost that scales linearly with system size, N , with a coefficient $\sim N_c N_b^3$, where N_c is a cluster size ~ 100 and N_b is the number of atomic states retained per site. The method is framed in real space, unlike DMFT. As a result it can capture the spatial amplitude and phase fluctuations on a specific lattice, or disordered background, or in the presence of a trap. It is also framed in 'real time', unlike QMC, and, as we will separately present, allows access to spectral information about the system.

We acknowledge use of the High Performance Computing Facility at HRI. Abhishek Joshi thanks the Infosys Foundation for support. AJ acknowledges fruitful discussions with Sauri Bhattacharyya, Arijit Dutta and Samrat Kadge.

Appendix A: Derivation of PSPA

$$Z = \int \prod_i D[\psi, \psi^*] D[b, \bar{b}] e^{-(S+S_b)}$$

Z_0 is the adiabatic partition function

$$Z_0 = \int D[b, \bar{b}] e^{-S} = \text{Tr}[\exp(-\beta H')]$$

e^{-S_b} is expanded to rewrite Z as

$$Z = \int D[\psi, \psi^*] D[b, \bar{b}] e^{-S} (1 - S_b + \frac{S_b^2}{2!} + \dots)$$

$$Z = \int D[\psi, \psi^*] Z_0 (1 - \frac{\int D[b, \bar{b}] e^{-S} S_b}{Z_0} + \frac{\int D[b, \bar{b}] e^{-S} S_b^2}{2! Z_0} + \dots)$$

$$\begin{aligned} S_b &= - \sum_{i,j,n \neq 0} t_{i,j} \bar{b}_n b_{j,n} - \sum_{i,j} B_{i,j} \bar{b}_{i,0} b_{j,0} \\ &= - \sum_{i,j,n} t_{i,j} \bar{b}_{i,n} b_{j,n} + \sum_{i,j} (t_{i,j} - B_{i,j}) \bar{b}_{i,0} b_{j,0} \end{aligned}$$

$$\beta X = \frac{\int D[b, \bar{b}] e^{-S} S_b}{Z_0}$$

X includes effects of zero frequency part of positive band

$$\begin{aligned} X &= \frac{\sum_{i \neq j} (t_{i,j} - B_{i,j}) \text{Tr}[e^{-\beta H'_i} b_i^\dagger] \text{Tr}[e^{-\beta H'_j} b_j]}{\text{Tr}[e^{-\beta H'_i}] \text{Tr}[e^{-\beta H'_j}]} \\ &- \sum_i B_{ii} (\sum_n e^{-\beta E_n^i} | \langle n | b_i^\dagger | n \rangle |^2 \end{aligned}$$

$$-\frac{1}{\beta} \sum_{n \neq m} \langle n | b_i^\dagger | m \rangle \langle m | b_i | n \rangle \frac{e^{-\beta E_n^i} - e^{-\beta E_m^i}}{(E_m^i - E_n^i)}$$

$$\beta Y = \frac{\int D[b, \bar{b}] e^{-S} S_b^2}{2! Z_0} - \frac{\beta^2 X^2}{2!} - (\text{small corr})$$

Y include second order correction due non zero frequency part of kinetic term. It has anomalous and normal contribution

$$Y = \sum_{i,j} t^2 / 2 (F1_{i,j;i,j+1} + F1_{i,j;i+1,j} + F2_{i,j;i+1,j} + F2_{i,j;i,j+1})$$

$|u\rangle, |v\rangle$ are eigenvector of H' at site index i, j $|p\rangle, |q\rangle$ are eigenvector of H' at site index k, m $F1$ is anomalous contribution at second order

$$F1_{i,j;k,m} = \sum_{\substack{u \neq v \\ p \neq q}} (\chi_{uvpq} + \bar{\chi}_{uvpq}) (A_{i,j;k,m}^{uvpq} + \frac{1}{4\beta} B_{i,j;k,m}'^{uvpq})$$

$$\begin{aligned} \chi_{uvpq} &= \langle u | b_{i,j}^\dagger | v \rangle \langle v | b_{i,j}^\dagger | u \rangle \langle p | b_{k,m} | q \rangle \\ &\langle q | b_{k,m} | p \rangle \end{aligned}$$

$$\begin{aligned} \bar{\chi}_{uvpq} &= \langle u | b_{i,j} | v \rangle \langle v | b_{i,j} | u \rangle \langle p | b_{k,m}^\dagger | q \rangle \\ &\langle q | b_{k,m}^\dagger | p \rangle \end{aligned}$$

$F2$ is normal contribution at second order

$$F2_{i,j;k,m} = \sum_{\substack{u \neq v \\ p \neq q}} (\chi'_{uvpq} + \bar{\chi}'_{uvpq}) (A_{i,j;k,m}^{uvpq} + \frac{1}{4\beta} B_{i,j;k,m}'^{uvpq})$$

$$\begin{aligned} \chi'_{uvpq} &= \langle u | b_{i,j}^\dagger | v \rangle \langle v | b_{i,j} | u \rangle \langle p | b_{k,m} | q \rangle \\ &\langle q | b_{k,m}^\dagger | p \rangle \end{aligned}$$

$$\begin{aligned} \bar{\chi}'_{uvpq} &= \langle u | b_{i,j} | v \rangle \langle v | b_{i,j}^\dagger | u \rangle \langle p | b_{k,m}^\dagger | q \rangle \\ &\langle q | b_{k,m} | p \rangle \end{aligned}$$

$$A_{i,j;k,m}^{uvpq} = \frac{e^{-\beta(\epsilon_q^{k,m} + \epsilon_v^{i,j})} - e^{-\beta(\epsilon_u^{i,j} + \epsilon_p^{k,m})}}{\epsilon_u^{i,j} + \epsilon_p^{k,m} - \epsilon_q^{k,m} - \epsilon_v^{i,j}} \text{ if } \text{den} \neq 0$$

$$\text{else } A_{i,j;k,m}^{uvpq} = \beta e^{-\beta(\epsilon_q^{k,m} + \epsilon_v^{i,j})}$$

$$B_{i,j;k,m}'^{uvpq} = \frac{e^{-\beta \epsilon_v^{i,j}} - e^{-\beta \epsilon_u^{i,j}}}{\epsilon_u^{i,j} - \epsilon_v^{i,j}} \frac{e^{-\beta \epsilon_q^{k,m}} - e^{-\beta \epsilon_p^{k,m}}}{\epsilon_q^{k,m} - \epsilon_p^{k,m}}$$

$$Z = \int D[\psi, \psi^*] e^{-\beta F} (1 - \beta X + \dots + \frac{\beta^2 X^2}{2!} + \beta Y + \dots + \text{higher order (diagrams+powers of } X \text{ and } Y))$$

$$Z \approx \int D[\psi, \psi^*] e^{-\beta(F+X-Y)}$$

$$F = -\frac{1}{\beta} \log(\text{Tr}[\exp(-\beta H')])$$

This is cumulant expansion. One exponentiate the series and we keep terms only till second order in the corrected free energy.

Appendix B: Approximate SPA functional at zero temperature

The full partition function is given by

$$Z_{SPA} = \int D[\psi, \psi^*] D[b, \bar{b}] e^{-S}$$

$$S = S_0 + S_{pert}$$

$$S_0 = \int_0^\beta d\tau [\sum_i \bar{b}_i (\partial_\tau - \mu) b_i + \psi_i^* \psi_i + \frac{U}{2} \bar{b}_i b_i (\bar{b}_i b_i - 1)]$$

$$S_{pert} = \int_0^\beta d\tau \sum_{ij} -C_{ij} (\bar{b}_i(\tau) \psi_j + h.c)$$

At zero temperature the minimum energy solution is where ψ is uniform. So we take $\psi_j = \psi$. Now

$$S_{pert} = \int_0^\beta d\tau \sum_i (-2\sqrt{t} \bar{b}_i(\tau) \psi_j + h.c)$$

$$\text{since } \sum_j C_{ij} = 2\sqrt{t}$$

$$Z_{SPA} = \int D[\psi, \psi^*] D[b, \bar{b}] e^{-S_0} (1 - S_{pert} + \frac{S_{pert}^2}{2!} + ..)$$

odd power in S_{pert} is zero due to number conservation. The cumulant expansion till fourth order and dropping higher order terms and exponentiating one gets

$$Z_{SPA}(T=0) \approx \int (d\psi d\psi^*)^N e^{-\beta E(\psi)}$$

$$\frac{E(\psi)}{N} = a_0 + a_2 |\psi|^2 + a_4 |\psi|^4$$

The ground state phase boundary is obtained by minimizing $E(\psi)$, where a_0 , a_2 and a_4 is defined in terms of atomic green function. N is the number of sites.

$$a_0 = [U/2n(n-1) - \mu n]$$

$$a_2 = (1 + 4t G_{ii}(0))$$

$$a_4 = -4t^2 G_{ii}^{2c}$$

$G_{ii}(0)$ and G_{ii}^{2c} is defined as below

$$G_{ii}(0) = \int_0^\beta d\tau - \langle T_\tau b(\tau) b^\dagger(0) \rangle$$

$$G_{ii}^{2c} = \int_0^\beta d\tau_1 d\tau_2 d\tau_3 - \langle T_\tau b(\tau_1) b(\tau_2) b^\dagger(0) b^\dagger(\tau_3) \rangle - 2\beta G_{ii}(0)^2$$

At zero the temperature SPA functional is same as the mean field functional

Appendix C: Approximate PSPA functional at zero temperature

The full partition function is given by

$$Z = \int \prod_i D[\psi, \psi^*] D[b, \bar{b}] e^{-(S_b + S_{pert} + S_b)}$$

At zero temperature the minimum energy solution is where ψ is uniform.

$$Z(T=0) = \int (d\psi d\psi^*)^N D[b, \bar{b}] e^{-S_0} (1 - (S_b + S_{pert}) + \frac{(S_b + S_{pert})^2}{2!} + \dots)$$

After integrating out bosons order by order one gets

$$= \int (d\psi d\psi^*)^N < e^{-S_0} > (1 + \frac{<S_{pert}^2>}{2!} + \frac{<S_{pert}^4>}{4!} + \frac{<S_b^2>}{2!} + \frac{<S_{pert}^2 S_b^2>}{4} + \text{higher order terms})$$

One can do cumulant expansion and drop higher terms. Above series can be approximated by

$$Z_{PSPA}(T=0) \approx \int (d\psi d\psi^*)^N e^{-\beta E_{corr}(\psi)}$$

$$E_{corr}(\psi) = E(\psi) + \delta E(\psi)$$

$$E(\psi) = -\frac{1}{\beta} (\log(e^{-<S_0>}) + \frac{<S_{pert}^2>}{2!} + \frac{<S_{pert}^4>}{4!})$$

$$\delta E(\psi) = -\frac{1}{\beta} (\frac{<S_b^2>}{2!} + \frac{<S_{pert}^2 S_b^2>}{4})$$

This is the approximated PSPA functional whose terms are explained as below

$$\frac{E_{corr}(\psi)}{N} = (a_0 + \delta a_0) + (a_2 + \delta a_2) |\psi|^2 + a_4 |\psi|^4$$

$$\frac{E(\psi)}{N} = (a_0) + (a_2) |\psi|^2 + a_4 |\psi|^4$$

where a_0 , a_2 , a_4 are described as in previous section.

$$\frac{\delta E(\psi)}{N} = \delta a_0 + \delta a_2 |\psi|^2$$

δa_0 and δa_2 are obtained from atomic green function

$$\delta a_0 = -\frac{2}{\beta} \int d\tau_1 d\tau_2 t^2 G_{ii}(\tau_1, \tau_2) G_{jj}(\tau_2, \tau_1)$$

$$\delta a_2 = -\frac{8}{\beta} (\int_0^\beta d\tau_1 d\tau_2 d\tau_3 d\tau_4 G^2(\tau_1, \tau_2; \tau_3, \tau_4) G(\tau_2, \tau_3) + G^2(i\omega_1 = 0, i\omega_2 = 0; i\omega_3 = 0, i\omega_4 = 0) G(i\omega_5 = 0, i\omega_6 = 0)) \frac{1}{\beta^2}$$

where G^2 is two particle green function given as below and G is single particle green function

$$G^2(\tau_1, \tau_2; \tau_3, \tau_4) = \langle T_\tau b(\tau_1) b(\tau_2) b^\dagger(\tau_3) b^\dagger(\tau_4) \rangle$$

$$G(\tau_1, \tau_2) = - \langle T_\tau b(\tau_1) b^\dagger(\tau_2) \rangle$$

The bosonic SPA is a ‘single site’ theory, albeit with a spatially correlated hybridisation field. The PSPA incorporates effects due to tunneling of particles to other sites. To lowest order PSPA corrects the $|\psi|^2$ term and leads to shifting of the phase boundary.

-
- ¹ M. Greiner, O. Mandel, T. Esslinger, T. W. Hänsch, and I. Bloch, *Nature (London)* **415**, 39 (2002).
- ² D. Clément, N. Fabbri, L. Fallani, C. Fort, and M. Inguscio, *Phys. Rev. Lett.* **102**, 155301 (2009).
- ³ P. T. Ernst, S. Götze, J. S. Krauser, K. Pyka, D. Lhmann, D. Pfannkuche and K. Sengstock, *Nature Physics* **6**, 56 (2010).
- ⁴ U. Bissbort, S. Götze, Y. Li, J. Heinze, J. S. Krauser, Malte Weinberg, C. Becker, K. Sengstock, and W. Hofstetter, *Phys. Rev. Lett.* **106**, 205303 (2011).
- ⁵ I. Bloch, *Nature Physics* **1**, 23 (2005).
- ⁶ I. Bloch, J. Dalibard, and W. Zwerger, *Rev. Mod. Phys.* **80**, 885 (2008).
- ⁷ B. Capogrosso-Sansone, S. G. Söyler, N. Prokof'ev, and B. Svistunov, *Phys. Rev. A*, **77**, 015602 (2008).
- ⁸ B. Capogrosso-Sansone, N. V. Prokof'ev, B. V. Svistunov, *Phys. Rev. B* **75**, 134302 (2007).
- ⁹ K. Sheshadri, H. R. Krishnamurthy, R. Pandit, T. V. Ramakrishnan, *Europhys. Letters*, **22**, (4), 257 (1993).
- ¹⁰ M. P. A. Fisher, P. B. Weichman, G. Grinstein, and D. S. Fisher, *Phys. Rev. B* **40**, 546 (1989).
- ¹¹ N. Elstner, H. Monien, *Phys Rev B* **59**, 12184 (1999).
- ¹² J. K. Freericks, H. Monien, *Europhys. Letters*, **26**, (7), 545 (1994).
- ¹³ F. E. A. dos Santos, A. Pelster, *Phys. Rev. A* **79**, 013614 (2009).
- ¹⁴ A. Dutta, C. Trefzger, and K. Sengupta, *Phys. Rev. B* **86**, 085140 (2012).
- ¹⁵ Dirk-Sren Lhmann *Phys. Rev. A* **87**, 043619
- ¹⁶ M. Knap, E. Arrigoni, and W. von der Linden, *Phys. Rev. B* **81**, 235122 (2010).
- ¹⁷ M. Knap, E. Arrigoni, and W. von der Linden, *Phys. Rev. B* **83**, 134507 (2011).
- ¹⁸ D. B. M. Dickerscheid, D. van Oosten, P. J. H. Denteneer, and H. T. C. Stoof, *Phys. Rev. A* **68**, 043623 (2003).
- ¹⁹ X. Lu, J. Li and Y. Yu, *Phys. Rev. A* **73**, 043607 (2006).
- ²⁰ A. S. Sajna, T. P. Polak, R. Micnas, and P. Rožek, *Phys. Rev. A* **92**, 013602 (2015).
- ²¹ K. Byczuk and D. Vollhardt, *Phys. Rev. B* **77**, 235106 (2008).
- ²² Wen-Jun Hu and Ning-Hua Tong, *Phys. Rev. B* **80**, 245110 (2009).
- ²³ P. Anders, E. Gull, L. Pollet, M. Troyer and Philipp Werner, *Phys. Rev. Lett.* **105**, 096402 (2010).
- ²⁴ D. Hügel and L. Pollet, *Phys. Rev. B* **91**, 224510 (2015).
- ²⁵ A. P. Kampf and G. T. Zimanyi, *Phys. Rev. B* **47**, 279 (1993).
- ²⁶ D. van Oosten, P. van der Straten, and H. T. C. Stoof, *Phys. Rev. A* **63**, 053601 (2001).
- ²⁷ K. Sengupta and N. Dupuis, *Phys. Rev. A* **71**, 033629 (2005).
- ²⁸ B. Lauritzen and J. W. Negele *Phys. Rev. C* **44**, 729
- ²⁹ B. Lauritzen and G. Bertsch *Phys. Rev. C* **39**, 2412
- ³⁰ H. Attias, Y. Alhassid *Nuclear Physics A* **625** (1997) 565-597
- ³¹ Daniele Malpetti and Tommaso Roscilde *Phys. Rev. Lett.* **119**, 040602